DEVELOPMENT OF COMPACT SELF-BALANCING ROBOT WITH SELF-STANDING AND STAIR-CLIMBING CAPABILITY

Dominic Robillard, Eric Lanteigne
E-mail: drobi062@uottawa.ca; Eric.Lanteigne@uottawa.ca

ABSTRACT

Self-balancing robots can turn on the spot using differential steering with better efficiency than tracked or four-wheel drive robots, and they can be many times their width in height. However they have two major limitations: they cannot stand-up on their own and cannot climb stairs. In this paper, a novel design is proposed to address these issues. A single degree of freedom is added to the center of a four-wheel drive robot. This arm allows the robot to climb stairs and stand-up on its own. A model and simulation of the balancing and the stair-climbing process are derived and the stair-climbing is compared against experimental results with a prototype. It was shown that the model closely follows the trend of the experimental results and provides a basis for future studies on the concept.

Keywords: robot; stair; climbing; balancing; standing.

DÉVELOPPEMENT D'UN ROBOT COMPACT S'AUTO-BALANÇANT AVEC HABILETÉ DE S'AUTO ÉRIGER ET DE MONTER DES ESCALIERS

RÉSUMÉ

Les robots qui s'auto-balançent peuvent tourner sur place en utilisant la traction différentielle avec une meilleure efficacité que les robots à chenilles ou à quatre roues. Ils peuvent être plusieurs fois leur largeur en hauteur. Cependant, ils ont deux limitations majeures : ils ne peuvent pas se lever eux-mêmes pour se balancer et ne peuvent pas monter des escaliers. Dans cet article, une nouvelle méthode est démontrée pour résoudre ces deux limitations : ajouter un bras avec un seul degré de liberté au centre d'un robot à quatre roues motrices. Ce bras permet au robot de monter des escaliers et de se lever soi-même. Un modèle et une simulation du balancement puis un modèle de la séquence pour monter une marche est développé. Le second modèle est comparé avec des résultats expérimentaux sur un prototype. Il a été montré que le modèle suit de près la tendance des résultats expérimentaux et fournit une base pour de futures études sur le concept.

Mots-clés : robot ; escaliers ; grimpe ; balance ; debout.

1. INTRODUCTION

Self-balancing robots are a special type of robotic platform that have a number of advantages. They have simple mechanical designs, where they do not require a steering mechanism which also makes them energy efficient. They can also turn on the spot and they have the ability to be taller without requiring a large base, which is closer to the human morphology. Those key advantages would make them perfect as surveillance robots if it was not for their two major limitations: they cannot stand up on their own and they cannot climb stairs. The objective of this research is to develop a simple and effective method to solve these two limitations. On the other hand, stair climbing robots tend to be bulky, expensive, and large which limits their ability to navigate door openings. They are often tracked drive robots which make them inefficient on flat ground. The robot proposed in this article is not only solving the two major limitations of self-balancing robots, but also proving that a very simple and compact design for stair-climbing is possible.

The most common configuration of stair-climbing robot is the tracked drive. Providing the threads are sufficiently long to overlap at least two steps at a time, the robot sees the staircase as a slope and can easily climb stairs. However the difficulty is in transitioning from a flat surface onto the first step. For this, several methods have been proposed. An example is the four-tracked robot that can move its front and rear tracks relative to each other to effectively climb the first step. Once the robot is on the first step, the robot can re-align its tracks and climb the remaining steps [1]. Another method is to use a deformable/reconfigurable track such as the LMA robot shown in [2]. Tracked robots have good outdoor applications but are not ideal for indoor robots because they consume a lot of energy, are slow, and are rather large.

The Whegs robots developed by the Case Western University [3] shows a good example of a biologically-inspired robot that is small, compact, and very good at climbing obstacles such as steps. These robots may however have trouble climbing a flight of stairs (more than one step) and because they do not have wheels, are less efficient on flat ground.

Self-balancing robots are in the category of differential drive robots. They have two wheels, but instead of a caster wheel they use a dynamic control loop to keep their body upright. Perhaps the best example of a commercially successful self-balancing platform is the Segway vehicle [4]. It is popular with tourists where they can rent them to visit local attractions.

The concept of self-balancing robots is not new [5], but the recent popularity of the Segway, the availability of low cost gyroscopic sensors, and powerful low-cost microcontrollers have inspired many versions of self-balancing robots both from research environments and amateurs. Good examples are given in [6–11].

Little work has been done on giving a self-balancing robot the ability to stand-up on its own. There is a lot of research done in the stand-up routine of humanoid robots [12] but they are not applicable since these platforms have legs with many degrees of freedom. Self-erecting an inverted pendulum has been examined, but the methods used (swing the pendulum back and forth from the hanging position until enough energy is provided to raise high) cannot be applied to self-balancing robots. One method is shown in [13] where an internal flywheel is forced to turn away from its spinning axis. The resulting precession force generated tilts the robot upwards until it is standing. The concept however requires at least two actuators (one to spin the disk, and the other to push the flywheel).

2. ROBOT OVERVIEW

The proposed solution is to have a four-wheel drive differential steering mobile platform. The left and right sides of the robot each have their own drive motors and both wheels on the same side are mechanically coupled. This platform provides good mobility on flat ground and is suitable for a self-balancing robot because the opposite wheel provides protection when the robot falls from balancing.

This platform is augmented with an arm attached at the middle of the body. This arm is driven by a powerful actuator and can indefinitely rotate around its joint. It is about twice as long as the body. The body

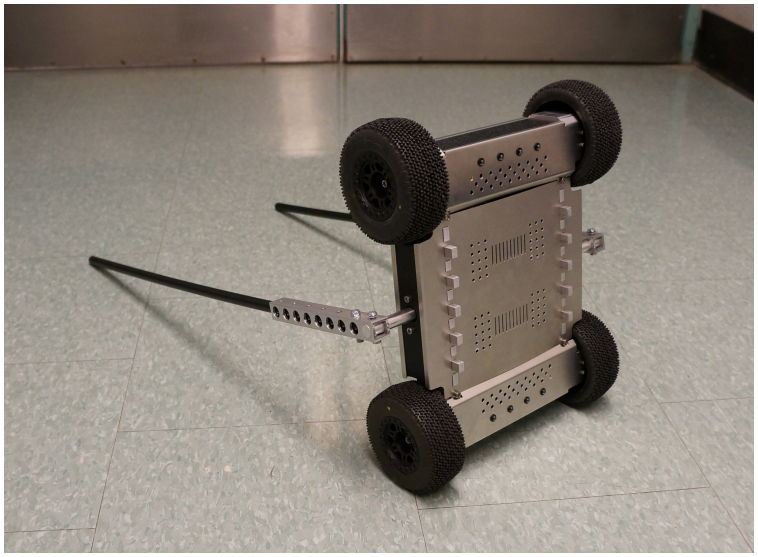

Fig. 1. Photograph of the robot developed for climbing stairs and self-balancing. Including its wheels, the standing robot is 14 inches high. The arm is 26 inches long.

carries all the heavy components while the arm is made as light as possible to keep the center of gravity of the robot predictable. Figure 1 shows a photograph of the custom made robot.

To stand-up from a resting position (four wheels in contact with floor), the arm rotates and lifts the body of the robot until close to equilibrium. At which point the balancing can start.

To climb stairs the robot aligns itself in four-wheel mode with the first step and the arm starts to rotate against the floor on the opposite side from the stairs. Once the arm touches the floor, the whole robot's body starts to turn. After ¼ turn, the body falls on the nose of the first step while the arm keeps rotating.

This process goes on for every step while the whole body of the robot continuously rotates. This is a simple effective method. It does have the drawback of making it more difficult to use sensors and cameras while the robot is climbing stairs. However because of the long arm towards the bottom of the stairs the climbing sequence is reliable. If the robot misses a step, it is almost impossible for the robot to tumble all the way down. The robot does not rely on the balancing ability while climbing steps.

In terms of the robot external dimensions, there are some guidelines that had to be followed. The wheel radius should not be more than the thread of a step and it should be at least large enough to grab the nose of a step with a vertical reaction force. This includes steps that have a fillet or chamfer to them. The dimension parameters such as the robot's body length, the robot's body width, and the rise of a step are all related. Essentially, the body of the robot must be kept smaller than the wheel radius to give a chance to properly grab the nose of a step.

The robot is also able to navigate down stairs, on slopes, and over random obstacles but the analysis of these manoeuvres is out of the scope of this paper.

3. MODEL

Because the design was an iterative process especially for the selection of motors and batteries, the model values below were first estimated before constructing the robot, and they were updated to reflect the real robot after it was finished. The robot parameters used in the models were measured from the prototype and are given by:

- $M = 5.012$ kg, total mass of robot (with arm and wheels).

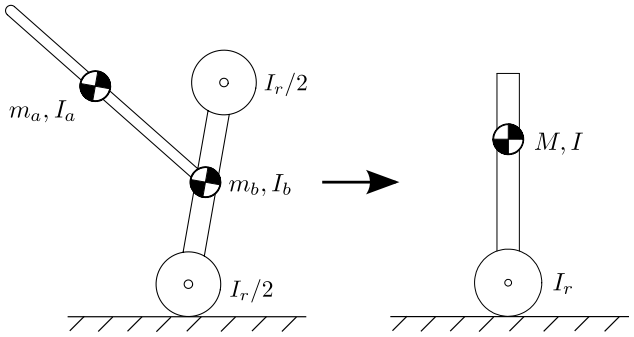

Fig. 2. The arm and the body are both combined into a single mass for the balance analysis (given that the arm is not rotating).

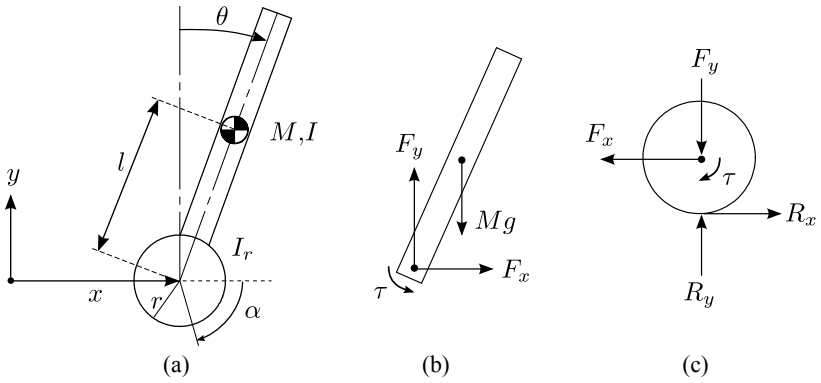

Fig. 3. (a) Nomenclature of the robot balancing; (b) forces acting on the robot's body; (c) forces acting on the robot's wheel. τ is the control input (torque between wheel and body)

- $r = 0.050$ m, wheel radius.
- $l = l_b = 0.127$ m, half of the distance wheel-to-wheel.
- $I = 0.056$ kg·m^2, robot's moment of inertia.
- $I_r = 0.001$ kg·m^2, rotational components's moment of inertia.

In Sections 3.1 and 3.2 we will derive the model for balancing and for stair-climbing respectively. These two models are unrelated as they are different scenarios. As such, the model derived in one scenario does not apply in the other. In Section 3.1 we will study the model and control of the balancing robot while it balances on flat ground. In Section 3.2 we will develop a model of the forces involved during the stair climbing process. The robot is not balancing while climbing stairs.

3.1. Model for Balancing and Controller Design

For the analysis of the balance, it is assumed that the arm is lumped with the body for simplification purposes. The top wheels are mechanically coupled to the bottom ones so their moment of intertia must be taken into account. As long as the arm does not rotate while balancing, the effect will be the same. If the arm is moving, it is simply considered as a disturbance. For the purpose of analyzing the balancing, the assumption is valid because the arm will not be moving. See Fig. 2.

The analysis will be made following the coordinate system shown in Fig. 3. The robot is broken down into two parts: the body and the wheel.

The position of the wheel is x. In the following equations the wheel is considered massless as its weight is included as part of the body weight M but it still has a mass moment of inertia I_r. This simplification is valid because the wheel is always at the same position relative to the body, but it can rotate relative to it. Applying Newton's second law of motion along x and y coordinates, and with moments along z on Fig. 3 we obtain:

$$I_r\ddot{\alpha} - \tau + Mr(\ddot{\alpha}r + \ddot{\theta}l\cos\theta - \dot{\theta}^2 l\sin\theta) = 0 \tag{1}$$

$$Mgl\sin\theta - \tau = I\ddot{\theta} + Ml^2\ddot{\theta} + Ml^2\dot{\theta}^2\sin^2\theta + Mlr\ddot{\alpha}\cos\theta - Ml^2\dot{\theta}\cos\theta\sin\theta \tag{2}$$

Because the robot is balancing, we assume its body angle θ is stable and is close to zero. Applying small angle approximations $\sin\theta \approx \theta$, $\cos\theta \approx 1$, and $\theta\dot{\theta}^2 \approx 0$ and re-arranging the equations we have:

$$C\ddot{\alpha} = (I + Ml^2 + Mlr)\tau - M^2gl^2r\theta \tag{3}$$

$$C\ddot{\theta} = Mgl(I_r + Mr^2)\theta - (I_r + Mlr + Mr^2)\tau \tag{4}$$

with: $C = IMr^2 + I_rMl^2 + II_r$

From where we write the state space representation as:

$$\dot{\mathbf{x}} = \mathbf{A}\mathbf{x} + \mathbf{B}u \tag{5}$$

with:

$$\mathbf{x} = \begin{Bmatrix} x_1 \\ x_2 \\ x_3 \\ x_4 \end{Bmatrix} = \begin{Bmatrix} \theta \\ \dot{\theta} \\ \alpha \\ \dot{\alpha} \end{Bmatrix}, \quad \mathbf{A} = \begin{bmatrix} 0 & 1 & 0 & 0 \\ \dfrac{Mgl(I_r + Mr^2)}{C} & 0 & 0 & 0 \\ 0 & 0 & 0 & 1 \\ -\dfrac{M^2gl^2r}{C} & 0 & 0 & 0 \end{bmatrix}, \quad \mathbf{B} = \begin{bmatrix} 0 \\ -\dfrac{I_r + Mlr + Mr^2}{C} \\ 0 \\ \dfrac{I + Ml^2 + Mlr}{C} \end{bmatrix}, \quad u = \tau$$

The control law for the robot's balancing is defined as:

$$u = -\mathbf{K}\mathbf{x} \tag{6}$$

where $\mathbf{K}$ needs to be determined. Here we will use the Linear Quadratic Regulator (LQR) method [14] to design an optimal controller. To do so, we define the performance index to be minimized as:

$$J = \int_0^\infty (\mathbf{x}\mathbf{Q}\mathbf{x} + Ru^2)dt \tag{7}$$

with $\mathbf{Q}$ and R being optimization parameters that need to be chosen. These values need to found by trial and error in the simulation, although as starting point, the Bryson's rule [15] can be applied. To minimize J we use the MATLAB® "lqr" function that takes as parameters the state space model and the $\mathbf{Q}$ and R constants. The "lqr" function returns $\mathbf{K}$ for the control law such that J is minimized. After several trials, the $\mathbf{Q}$ and R parameters that gave a satisfactory response are:

$$\mathbf{Q} = \begin{bmatrix} 0 & 0 & 0 & 0 \\ 0 & 0 & 0 & 0 \\ 0 & 0 & 20 & 0 \\ 0 & 0 & 0 & 1 \end{bmatrix}, \text{ and } R = 0.5 \tag{8}$$

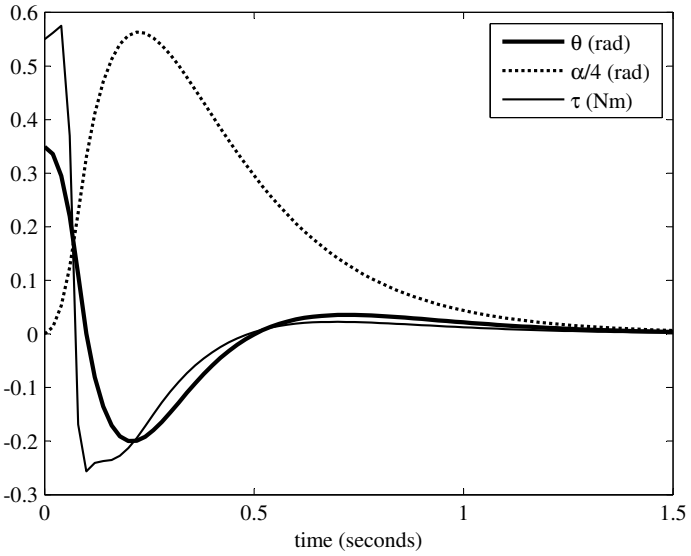

Fig. 4. Simulation of the robot recovering from a 20º disturbance while balancing. The simulation is run with the discrete controller and the nonlinear model of the robot. Sampling rate is 50Hz.

for which the "lqr" function returns:

$$\mathbf{K} = \begin{bmatrix} -101.2 & -15.11 & -6.325 & -3.343 \end{bmatrix} \tag{9}$$

Since the robot is controlled with a microcontroller, the model needs to be converted to a discrete model. The continuous state space model was converted to a discrete state space model using the MATLAB® "c2d" function and a new discrete $\mathbf{K}_d$ was computed using the "dlqr" function. We obtained for a sample rate of 50Hz:

$$\mathbf{K}_d = \begin{bmatrix} -11.07 & -1.473 & -0.5405 & -0.2960 \end{bmatrix} \tag{10}$$

It is also desirable for testing to have a nonlinear model of the robot. Some control systems will work with a linear model but are unstable with the nonlinear version. The control system cannot easily be designed from the nonlinear version, but offers a good validation tool. Re-arranging Eqs. (1) and (2) by extracting $\ddot{\alpha}$ and $\ddot{\theta}$ we obtain the nonlinear equations:

$$\ddot{\alpha} = \frac{\sin\theta(rM^2l^3\dot{\theta}(\dot{\theta}\cos\theta\sin\theta + \dot{\theta} - \cos^2\theta) - grM^2l^2\cos\theta + lrMl\dot{\theta}^2) + (Ml^2 + rMl\cos\theta + I)\tau}{M^2l^2r^2\sin^2\theta + I_rMl^2 + lMr^2 + II_r} \tag{11}$$

$$\ddot{\theta} = \frac{\begin{array}{c}\sin\theta(M^2lr^2\dot{\theta}(l\dot{\theta}\sin\theta - g - l\dot{\theta}\cos\theta + l\cos\theta) + MlI_r(l\dot{\theta}^2\sin\theta + l\dot{\theta}\cos\theta - g)) \\ +(Mr^2 - Mlr\cos\theta + I_r)\tau\end{array}}{M^2l^2r^2\sin^2\theta + I_rMl^2 + lMr^2 + II_r} \tag{12}$$

A discrete model was written and the nonlinear model was augmented with the Pittman GM9236 motor model. It ensures that the current control law is compatible with the real torque limited motors. Figure 4 shows the simulation results for the pendulum subjected to a 20° disturbance. The system successfully recovers in about one second. The settling time could be shorter but then vibrations started to appear on the real model.

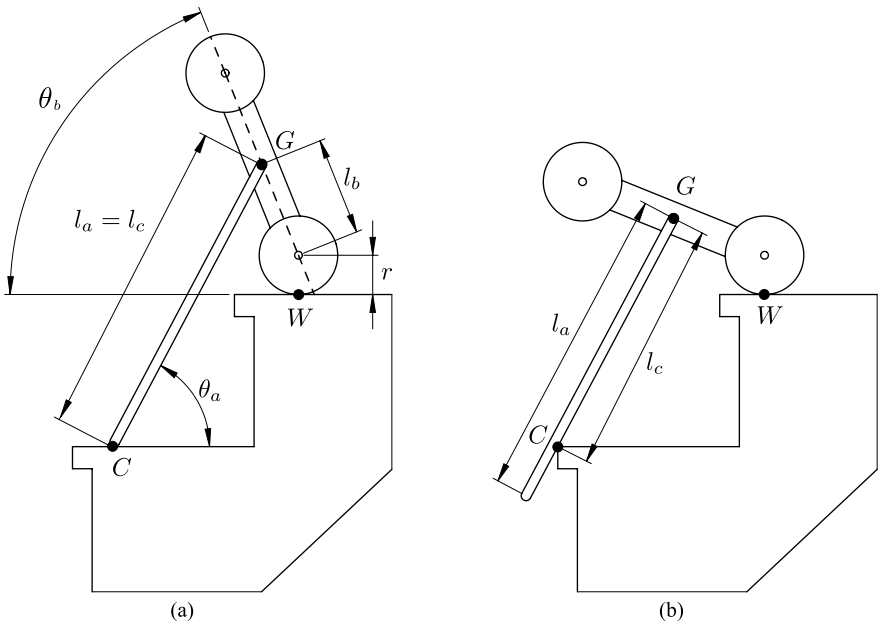

Fig. 5. Schematic of the two cases encountered during the stair-climbing process. (a) Case A: the tip of the arm is in contact with a horizontal surface; (b) case B: the arm is in contact with the nose of a step.

3.2. Model for Stair Climbing

In this section a new model for the robot climbing stairs will be developed. The robot is not balancing while climbing stairs, thus the model developed in Section 3.1 is not applicable here.

During the stair climbing sequence, the robot relies on the friction of the wheel to overcome the normal forces generated by the arm against the steps, and the sliding friction force of the arm. The stair-climbing process can be simplified to have only two different configurations that we call case A and case B. This is a simplification as there exists other configurations (such as when the body of the robot is touching the step instead of the wheels), however these cases are not considered critical due to lower forces involved. Figure 5 shows the two configurations that were analyzed. Figure 6 shows the forces for both cases on the arm and the robot's body.

It is assumed that the robot is currently going upstairs. There is a sliding motion of the arm's contact point and the wheels of the robot are not slipping. A slipping condition would occur whenever force W_x is higher

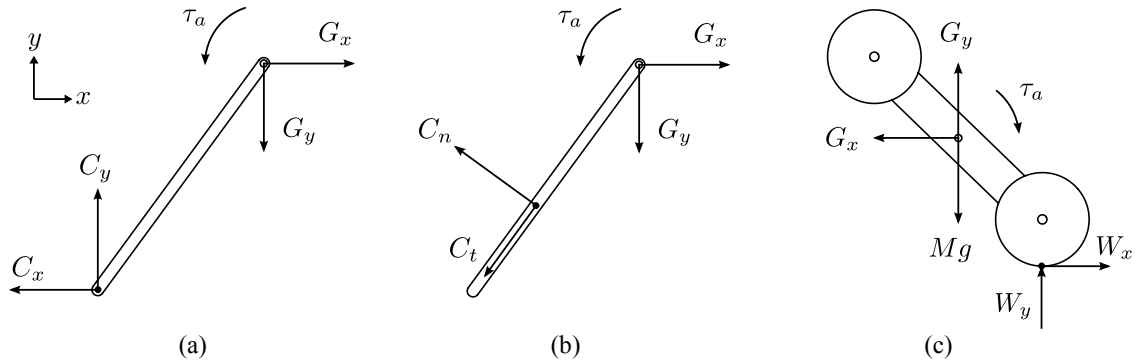

Fig. 6. Free body diagrams of the arm and the robot's body. (a) Forces applied on the arm under case A; (b) forces applied on the arm under case B; (c) forces applied on the robot's body for both case A and case B.

than the friction force the wheel can provide. The arm length was determined such that this never occurs in real stair conditions with a safety factor of at least 2. The condition is:

$$W_x < \mu_w W_y \tag{13}$$

where μ_w is the coefficient of friction between the wheel and the step surface. Also for case A:

$$C_x = \mu_c C_y \tag{14}$$

where μ_c is the coefficient of friction of the arm at its contact point. And for case B:

$$C_t = \mu_c C_n \tag{15}$$

Case B can be re-written to be compatible with the equations of case A by transforming C_n and C_t into C_x and C_y. Then we have:

$$C_x = \begin{cases} \mu_x C_y & \text{if case A} \\ C_n(\sin\theta_a + \mu_c \cos\theta_a) & \text{if case B} \end{cases} \tag{16}$$

$$C_y = \begin{cases} C_y & \text{if case A} \\ C_n(\cos\theta_a - \mu_c \sin\theta_a) & \text{if case B} \end{cases} \tag{17}$$

Applying sum of forces on the arm and body, we obtain a set of equations that can be solved to obtain the arm and wheel torques (the wheel torque is defined as $\tau_w = rW_x$), as a function of the arm angle θ_a, body angle θ_b, and contact length l_c. For case A we obtain:

$$\tau_a = \frac{Mgl_b l_c \cos\theta_b(\cos\theta_a + \mu_c \sin\theta_a)}{D} \tag{18}$$

$$\tau_w = \frac{Mgl_b \mu_c r \cos\theta_b}{D} \tag{19}$$

with: $D = l_b \cos\theta_b - \mu_c r + l_c \cos\theta_A - l_b \mu_c \sin\theta_b + l_c \mu_c \sin\theta_a$.

For case B we obtain:

$$\tau_a = \frac{Mgl_b l_c \cos\theta_b}{E} \tag{20}$$

$$\tau_w = \frac{Mgl_b r(\sin(\theta_a - \theta_b) + \mu_c \cos(\theta_a - \theta_b) + \sin(\theta_a + \theta_b) + \mu_c \cos(\theta_a + \theta_b))}{2E} \tag{21}$$

with: $E = l_b \cos(\theta_a + \theta_b) - l_b \mu_c \sin(\theta_a + \theta_b) - r\sin\theta_a + l_c - \mu_c r \cos\theta_a$

4. STAIR-CLIMBING RESULTS

To validate the theory of Section 3.2, the experimental results of the robot climbing a complete step were obtained. Figure 7 shows a sequence of photographs taken during the experiment.

To avoid dynamic effects, the experiment was conducted at a slow rate where the arm was rotating at a speed of about one degree per second. While the experiment was performed, the robot's internal circuitry recorded a number of parameters into a memory card which could then be analyzed offline. For this experiment, the robot logged the following parameters:

- Current time: time was synchronized with the camera's internal time. This allows matching the photographs with the readings in the memory card.

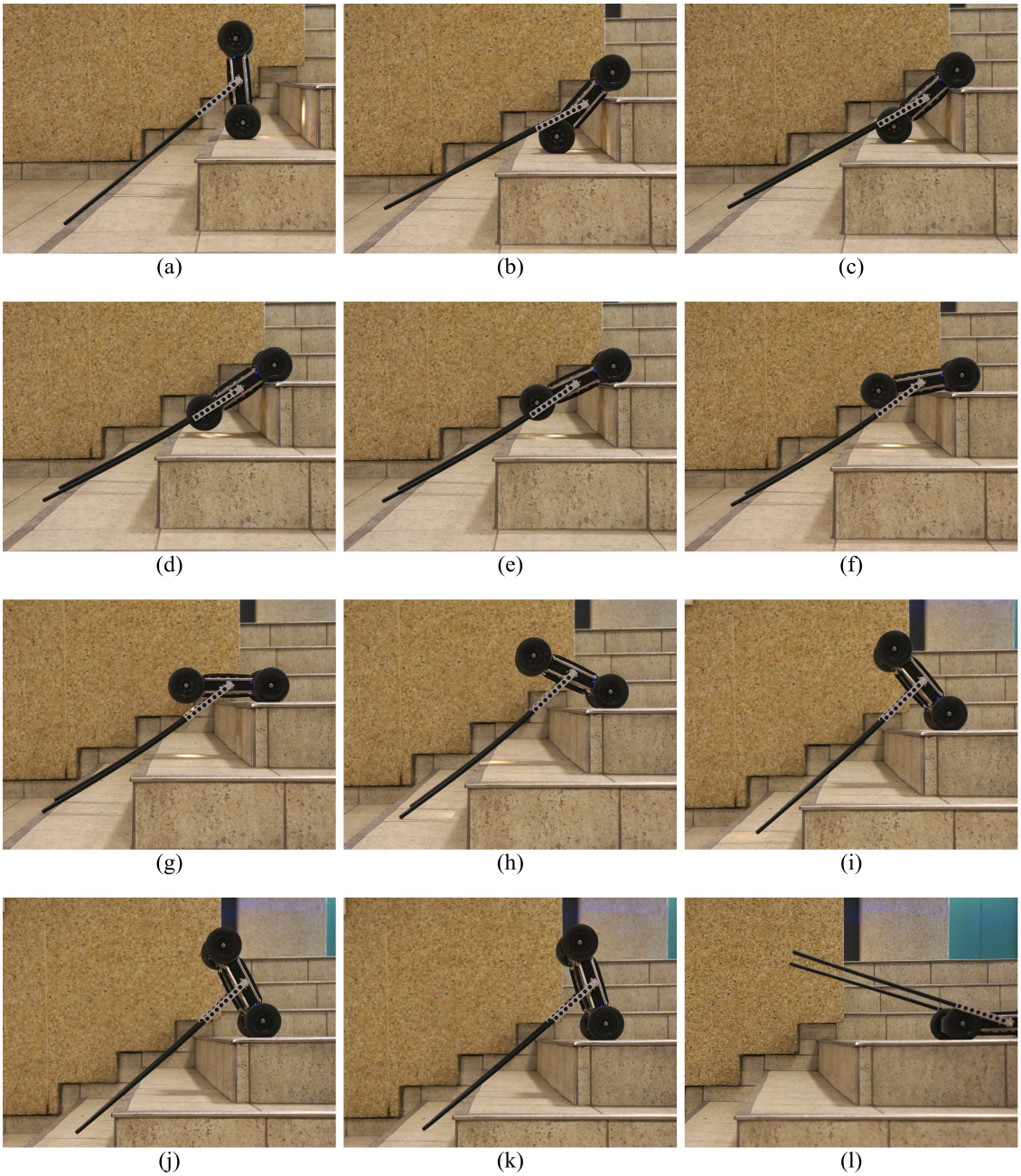

Fig. 7. Sequenced photographs of the robot climbing a single step. The robot starts with its body in a vertical position (a) and finishes at the same position (upside down) on the next step after (k). The same sequence would be repeated for more steps.

- Inertial measurements: the gyroscope and accelerometer readings were recorded to ensure the events on the pictures are well synchronized.
- Motor currents: drive motors and arm motor.
- Battery voltage.

The arm angle θ_a, body angle θ_b, and arm contact length $l_c$were measured using pixel coordinates from the photographs. Whether the robot was in case A or case B was also determined from the picture. The arm an body angles could have also been determined by the logged measurements in the memory card, but were less accurate then measuring on the picture. Referring to Fig. 7, the contact mode is as follow:

- (a): Just before being vertical, the robot is finishing its previous cycle.
- (b): The robot has fallen down with body against step. The arm is raised.
- (c): Arm pushes lightly on the bottom step. Body slipped until the wheel grabs the step run.
- (d) to (f): Case B: the bottom wheel has lifted from the step.
- (g) to (h): Case A: the arm is now pushing against the run of the step
- (i) to (k): Case B.
- (l): The robot passes its equilibrium point and falls (ready for another step).

Once θ_a, θ_b, l_c, and the mode were determined using the photographs, the theoretical torque values were calculated using Eqs. (18–21). The arm coefficient of friction μ_a was assumed to be 0.25 (arm is made of acetal). The logged motor currents were converted to torques using the motor's models. For the arm drivetrain, an estimated efficiency of 0.8 was assumed to account for the triple stage greased planetary gearbox and the chain drive in the arm mechanism. Figures 8 and 9 show a graphical representation of the results for the arm and wheel torques. The annotations refer to the pictures in Fig. 7.

For both figures, we see that the trend is closely followed between both theoretical and experimental data. The torque values are about zero when the body is vertical. This is expected because the center of gravity of the robot is directly above its wheels and the arm does not need to apply any torque. There is discrepancy between the model and the real data for point (b) for the arm torque. It is because the model assumes the bottom wheel is not touching the ground while in reality it is still in contact with it, thus the lower arm torque required. For the wheel torque, point (c) is peaking to almost one Nm, which can happen if the robot tries to move forward but is blocked by the body in contact with the riser (see Fig. 7 (c)).

There are a number of sources of errors. For one, the arm gearbox efficiency and the arm coefficient of friction were assumed based on literature examples but were not explicitly available. Other modelling errors could be possible. Dynamic effects were neglected, although the experiment was conducted at very slow speed. Angle and distance measurements on the photographs are subjected to resolution, visual, and lens distortion errors. The current sensors have an error of ±1.5% plus the error due to the digital-to-analog converter resolution and noise. There are also unmodeled physical properties such as friction, arm bending, wheel deformation, motor dead-band, and backlash. Nonetheless with all these sources of error, it is clear that the model is closely following the experimental data.

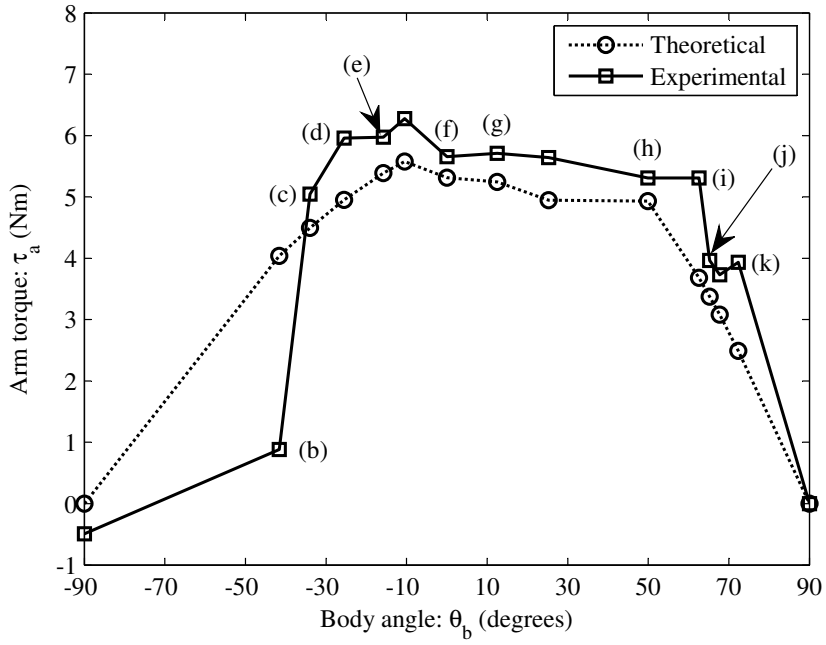

Fig. 8. Torque exerted on the arm of the robot during the climbing sequence shown in Fig. 7.

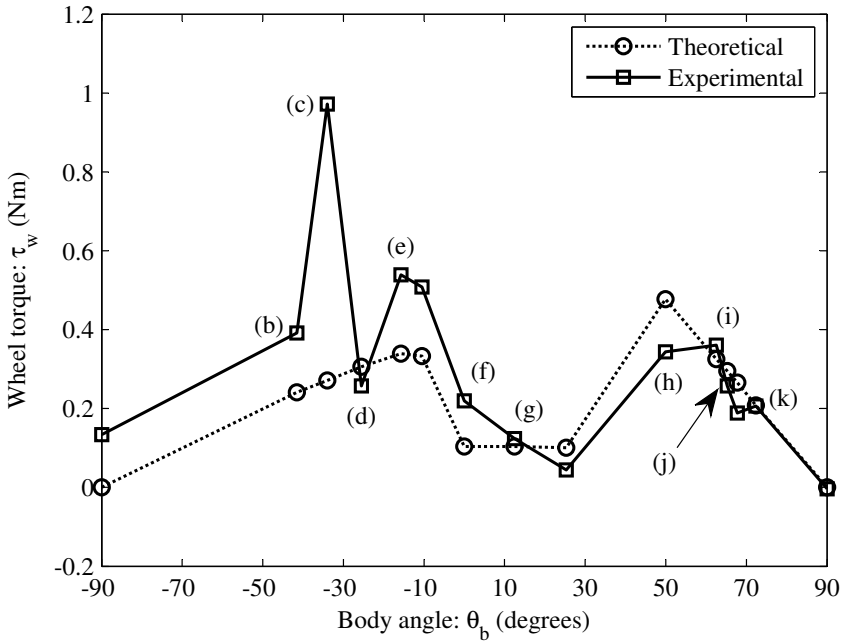

Fig. 9. Torque exerted on the wheels of the robot during the climbing sequence shown in Fig. 7.

5. CONCLUSIONS

In this paper, a simple and effective design that gives self-balancing robots the ability to stand-up and climb obstacles such as stairs was proposed, developed, and tested. An overview of the concept and the design of the balancing control loop were covered, and a model for the analysis of the stair-climbing torques in both the arm and the wheels was developed. This new stair-climbing model was then validated using experimental data on the real robot. We showed that the addition of two long arms in the center of a four-wheel drive robot allows it to stand-up for balancing and navigate stairs. The single extra degree of freedom (for a total of three counting the drive train) increases the field capabilities of self-balancing robots.

REFERENCES

1. Vu, Q.H., Kim, B.S. and Song, J.B. "Autonomous stair climbing algorithm for a small four-tracked robot." In "International Conference on Control, Automation and Systems, 2008. ICCAS 2008," pp. 2356–2360. doi: 10.1109/ICCAS.2008.4694199, October 2008.
2. Ben-Tzvi, P., Ito, S. and Goldenberg, A. "Autonomous stair climbing with reconfigurable tracked mobile robot." In "International Workshop on Robotic and Sensors Environments, 2007. ROSE 2007," pp. 1–6. doi: 10.1109/ROSE.2007.4373976, October 2007.
3. Taylor, B.K., Balakirsky, S., Messina, E. and Quinn, R.D. "Modeling, validation and analysis of a whegs robot in the USARSim environment." In "Proceedings of SPIE 6962, Unmanned Systems Technology X, 69621B," pp. 69621B–69621B. doi:10.1117/12.777604, April 2008.
4. "Segway – the leader in personal, green transportation." `http://www.segway.com/`, November 2012.
5. Yamafuji K., Feng M. Q., K.T. "Robots driven by parallel bicycles." *International Journal of Mechanics and Control*, Vol. 9, No. 2, pp. 3–11, 2008.
6. Jeong, S. and Takahashi, T. "Wheeled inverted pendulum type assistant robot: design concept and mobile control." *Intelligent Service Robotics*, Vol. 1, No. 4, pp. 313–320. ISSN 1861-2776, 1861-2784. doi:10.1007/s11370-008-0024-5, October 2008.
7. Tang, R. and Green, R. "Obstacle avoidance on a mobile inverted pendulum robot." In "Image and Vision Computing New Zealand, 2009. IVCNZ '09. 24th International Conference," pp. 254 –259. doi: 10.1109/IVCNZ.2009.5378400, November 2009.
8. Anderson, D.P. "nBot, a two wheel balancing robot." `http://www.geology.smu.edu/dpa-www/robo/nbot/`, November 2012.
9. Feng, T., Liu, T., Wang, X., Xu, Z., Zhang, M. and Han, S.c. "Modeling and implementation of two-wheel self-balancing robot equipped with supporting arms." In "2011 6th IEEE Conference on Industrial Electronics and Applications (ICIEA)," pp. 713 –718. doi:10.1109/ICIEA.2011.5975678, June 2011.
10. Takei, T., Imamura, R. and Yuta, S. "Baggage transportation and navigation by a wheeled inverted pendulum mobile robot." *IEEE Transactions on Industrial Electronics*, Vol. 56, No. 10, pp. 3985 –3994. ISSN 0278-0046. doi:10.1109/TIE.2009.2027252, October 2009.
11. Kumagai, M. and Ochiai, T. "Development of a robot balancing on a ball." In "International Conference on Control, Automation and Systems, 2008. ICCAS 2008," pp. 433 –438. doi:10.1109/ICCAS.2008.4694680, October 2008.
12. Chen, C.Y., Shih, B.Y., Shih, C.H. and Wang, L.H. "Enhancing robust and stability control of a humanoid biped robot: system identification approach." *Journal of Vibration and Control*. ISSN 1077-5463, 1741-2986. doi:10.1177/1077546312442947, April 2012.
13. Miao, S. and Cao, Q. "Modeling of self-tilt-up motion for a two-wheeled inverted pendulum." *Industrial Robot: An International Journal*, Vol. 38, No. 1, pp. 76–85. ISSN 0143-991X. doi:10.1108/01439911111097878, January 2011.
14. Stefani, R.T., Shahian, B., Savant, C.J. and Hostetter, G.H. *Design of Feedback Control Systems*. 4 ed.. Oxford University Press, USA. ISBN 0195142497, August 2001.
15. Jr, A.E.B. and Ho, Y.C. *Applied Optimal Control: Optimization, Estimation, and Control*. Hemisphere Publishing Company. ISBN 9780891162285, 1975.